NUMERICAL SIMULATIONS OF WOVEN COMPOSITE MATERIALS WITH VOXEL-FE MODELS

G. Hello*[1], J. Schneider[2], Z. Aboura[3]

[1] *UFR Sciences et Technologies, Laboratoire de Mécanique et d'Energétique d'Evry, Université d'Evry Val d'Essonne, 40 Rue du Pelvoux - 91020 Courcouronnes - France*
[2] *Snecma - Safran Group, Site de Villaroche, Rond-point René Ravaud - Réau - 77550 Moissy-Cramayel - France*
[3] *Laboratoire Roberval - CNRS UMR 7337, Université de Technologie de Compiègne, Centre de Recherches de Royallieu - BP 20529 - 60205 Compiègne Cedex - France*
* *Corresponding Author: gaetan.hello@ufrst.univ-evry.fr*

Keywords: woven composites, numerical homogenization, voxel-FE meshes

Abstract

A procedure for the determination of homogenized elastic moduli from a voxel-FE description of the material architecture is presented. The voxel-FE approach enables the automated and robust generation of Representative Elementary Volumes for a wide range of heterogeneous materials, in particular woven composites. Thanks to the regularity of boundary meshes in voxel models, the application of boundary conditions (periodic, kinematic uniform, static uniform and mixed-uniform) as well as the determination of volumic averages for stresses and strains can be both performed easily and efficiently. The convergence of voxel-FE results and the influence of boundary conditions are studied for two typical problems.

1. Introduction

The inherent complexity of woven composite materials requires the development of specific modelisation strategies and softwares such as Wisetex [1, 2] or Texgen [3]. The noticeable difference in behaviors encountered on the heterogeneous micro-scale and the macro-scale is strongly related to the geometric architecture of the material. The simulation of woven composites thus requires to handle efficiently complex geometric information in order to generate representative FE-models. The authors have developed a modelisation approach and a related software based on voxel finite elements [4, 5, 6]. The basis of this approach has been used extensively during the past 20 years in order to represent heterogeneous material architectures [7, 8]. However, the genericity of the authors' specific voxel-FE approach enables to generate automatically FE-models (fig. 1) for potentially any kind of material architectures (polycrystalline aggregates, woven composites, particles reinforced composites...). This approach has the main interests of its user-friendliness, robustness, high automation level, genericity and natural relation with tomographic data. Nonetheless, the size of voxel-FE models is generally higher than the one of classical models and the use of regular hexahedral elements does not enable direct accurate stress/strain estimations near materials interfaces. The first drawback can be mitigated by the fact that simulations involving millions of degrees of freedom can now

be performed rapidly on affordable modern computers. About the second one, very accurate stress/strain evaluations do not matter when looking for homogenized properties.

This presentation will address the specific topic of the numerical homogenization of elastic properties for mesoscopic Representative Elementary Volumes described with voxel-FE models. The effects of elements size and boundary conditions are more particularly studied.

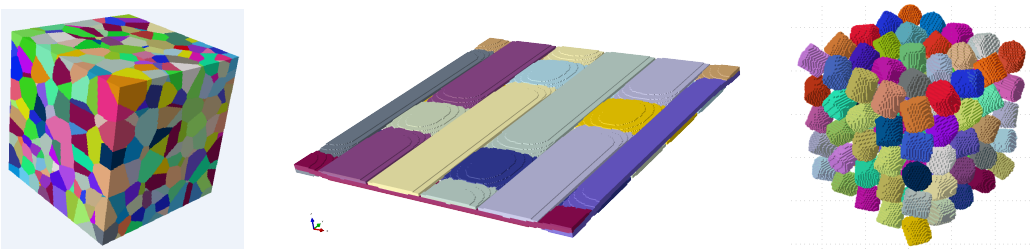

Figure 1. Voxel-FE models: (left) metallic polycrystalline aggregate, (center) satin-5 woven composite, (right) particle reinforced metal matrix composite.

2. Numerical homogenization of elastic properties

2.1. Principles

Here, we assume that the material mesoscopic properties are correctly described statistically speaking by the hexahedral REV Ω defined as:

$$\Omega = \left[x_1^0, x_1^0 + L_1\right] \times \left[x_2^0, x_2^0 + L_2\right] \times \left[x_3^0, x_3^0 + L_3\right] \tag{1}$$

where $\left(x_1^0, x_2^0, x_3^0\right)$ is the origin of the REV and (L_1, L_2, L_3) are the lengths in the different directions.

In Ω, the material constitutive law C_{ijkl} depends on the position $\mathbf{x}$ inside the REV. The local stress and strain states are then related according to:

$$\sigma_{ij}(\mathbf{x}) = C_{ijkl}(\mathbf{x}) \cdot \varepsilon_{kl}(\mathbf{x}) \tag{2}$$

If we define the spatial averages of local stress and strain by:

$$\left\langle \sigma_{ij} \right\rangle = \frac{1}{|\Omega|} \int_\Omega \sigma_{ij}(\mathbf{x})\ dV \qquad \left\langle \varepsilon_{ij} \right\rangle = \frac{1}{|\Omega|} \int_\Omega \varepsilon_{ij}(\mathbf{x})\ dV \tag{3}$$

Then, the macroscopic apparent material constitutive law C^*_{ijkl} relates $\left\langle \sigma_{ij} \right\rangle$ with $\langle \varepsilon_{kl} \rangle$:

$$\left\langle \sigma_{ij} \right\rangle = C^*_{ijkl} \cdot \langle \varepsilon_{kl} \rangle \tag{4}$$

The purpose of the numerical homogenization procedure is the determination of the different coefficients in C^*_{ijkl}. From now on, it will be assumed that the homogenized material behavior may be accurately described using a 3D orthotropic law with 9 parameters.

2.2. Types of Boundary Conditions

Once the REV geometric and material properties have been correctly described in a FE model, calculations with different boundary conditions are successively run in order to gain enough information for the identification of material parameters. For the 3D orthotropic case, at least 6 different load-cases need to be successively applied. These load-cases can be derived from different sets of boundary conditions.

2.2.1. Kinematic Uniform Boundary Conditions

The REV is here submitted to an imposed displacement field on its boundary:

$$u_i(\mathbf{x}) = \varepsilon^0_{ij} \cdot x_j(\mathbf{x}) \quad , \quad \forall \mathbf{x} \in \partial\Omega \tag{5}$$

In that case we have:

$$\left\langle \varepsilon_{ij} \right\rangle = \varepsilon^0_{ij} \tag{6}$$

The results of FE simulations will lead to the evaluation of $\left\langle \sigma_{ij} \right\rangle$. Material coefficients are then identified according to Eq. 4.

2.2.2. Static Uniform Boundary Conditions

The REV is here submitted to an imposed traction field on its boundary:

$$t_i(\mathbf{x}) = \sigma^0_{ij} \cdot n_j(\mathbf{x}) \quad , \quad \forall \mathbf{x} \in \partial\Omega \tag{7}$$

In that case we have:

$$\left\langle \sigma_{ij} \right\rangle = \sigma^0_{ij} \tag{8}$$

The results of FE simulations will lead to the evaluation of $\left\langle \varepsilon_{ij} \right\rangle$ that will then be used to identify materials coefficients according to $\left\langle \varepsilon_{ij} \right\rangle = S^*_{ijkl} \cdot \langle \sigma_{kl} \rangle$ (with $C^*_{ijkl} = \left(S^*_{ijkl}\right)^{-1}$). Practically, Dirichlet boundary conditions must also be imposed in order to avoid rigid-body motions.

2.2.3. Periodic Mixed Uniform Boundary Conditions

These boundary conditions can be seen as an orthogonal mix of SUBC and KUBC:

$$\left(u_i(\mathbf{x}) - \varepsilon^0_{ij} \cdot x_j(\mathbf{x})\right) \cdot \left(t_i(\mathbf{x}) - \sigma^0_{ij} \cdot n_j(\mathbf{x})\right) = 0 \quad , \quad \forall \mathbf{x} \in \partial\Omega \tag{9}$$

They enforce a spacial averaged strain on the RVE:

$$\left\langle \varepsilon_{ij} \right\rangle = \varepsilon^0_{ij} \tag{10}$$

There is not unicity of the MUBC. Among the possible choices, Pahr and Zysset [9] proposed the so called Periodic-MUBC that can provide accurate results for periodic REV (tab. 1). By definition, $\partial\Omega^{\pm}_i$ is the face of the hexahedral REV which has the outward normal $\pm\mathbf{e}_i$.

$\left\langle \varepsilon_{ij} \right\rangle = \varepsilon^0_{ij}$	$\partial\Omega_1^+$	$\partial\Omega_1^-$	$\partial\Omega_2^+$	$\partial\Omega_2^-$	$\partial\Omega_3^+$	$\partial\Omega_3^-$
$\mathbf{e}_1 \otimes \mathbf{e}_1$	$u_1 = L_1$ $t_2 = t_3 = 0$	$u_1 = 0$ $t_2 = t_3 = 0$	$u_2 = 0$ $t_1 = t_3 = 0$	$u_2 = 0$ $t_1 = t_3 = 0$	$u_3 = 0$ $t_1 = t_2 = 0$	$u_3 = 0$ $t_1 = t_2 = 0$
$\mathbf{e}_2 \otimes \mathbf{e}_2$	$u_1 = 0$ $t_2 = t_3 = 0$	$u_1 = 0$ $t_2 = t_3 = 0$	$u_2 = L_2$ $t_1 = t_3 = 0$	$u_2 = 0$ $t_1 = t_3 = 0$	$u_3 = 0$ $t_1 = t_2 = 0$	$u_3 = 0$ $t_1 = t_2 = 0$
$\mathbf{e}_3 \otimes \mathbf{e}_3$	$u_1 = 0$ $t_2 = t_3 = 0$	$u_1 = 0$ $t_2 = t_3 = 0$	$u_2 = 0$ $t_1 = t_3 = 0$	$u_2 = 0$ $t_1 = t_3 = 0$	$u_3 = L_3$ $t_1 = t_2 = 0$	$u_3 = 0$ $t_1 = t_2 = 0$
$\mathbf{e}_1 \otimes \mathbf{e}_2$ $+\mathbf{e}_2 \otimes \mathbf{e}_1$	$u_2 = L_1$ $t_1 = u_3 = 0$	$u_2 = 0$ $t_1 = u_3 = 0$	$u_1 = L_2$ $t_2 = u_3 = 0$	$u_2 = 0$ $t_2 = u_3 = 0$	$u_3 = 0$ $t_1 = t_2 = 0$	$u_3 = 0$ $t_1 = t_2 = 0$
$\mathbf{e}_1 \otimes \mathbf{e}_3$ $+\mathbf{e}_3 \otimes \mathbf{e}_1$	$u_3 = L_1$ $t_1 = u_2 = 0$	$u_3 = 0$ $t_1 = u_2 = 0$	$u_2 = 0$ $t_1 = t_3 = 0$	$u_2 = 0$ $t_1 = t_3 = 0$	$u_1 = L_3$ $u_2 = t_3 = 0$	$u_1 = 0$ $u_2 = t_3 = 0$
$\mathbf{e}_2 \otimes \mathbf{e}_3$ $+\mathbf{e}_3 \otimes \mathbf{e}_2$	$u_1 = 0$ $t_2 = t_3 = 0$	$u_1 = 0$ $t_2 = t_3 = 0$	$u_3 = L_2$ $u_1 = t_2 = 0$	$u_3 = 0$ $u_1 = t_2 = 0$	$u_2 = L_3$ $u_1 = t_3 = 0$	$u_2 = 0$ $u_1 = t_3 = 0$

Table 1. PMUBC boundary conditions for the 6 load cases applied to the hexahedral REV Ω, adapted from [9].

2.2.4. Periodic Boundary Conditions

In the case of woven composite materials, the periodicity of the architecture authorizes the use of PBC. These boundary conditions impose a linear relation between displacements on opposite faces:

$$u_i^{\partial\Omega_k^+}(\mathbf{x} + L_k \cdot \mathbf{e}_k) - u_i^{\partial\Omega_k^-}(\mathbf{x}) = \varepsilon^0_{ij} \cdot \left(x_j^{\partial\Omega_k^+}(\mathbf{x} + L_k \cdot \mathbf{e}_k) - x_j^{\partial\Omega_k^-}(\mathbf{x}) \right) \quad , \quad \forall \mathbf{x} \in \partial\Omega_k^-, k \in \{1,2,3\} \tag{11}$$

This leads to:

$$\left\langle \varepsilon_{ij} \right\rangle = \varepsilon^0_{ij} \tag{12}$$

2.3. Elastic properties bounding

The SUBC and KUBC solutions provide a bounding of effective properties:

$$\left(S^{SUBC}_{ijkl} \right)^{-1} \leq C^*_{ijkl} \leq C^{KUBC}_{ijkl} \tag{13}$$

MUBC properties are bounded the same way:

$$\left(S^{SUBC}_{ijkl} \right)^{-1} \leq C^{MUBC}_{ijkl} \leq C^{KUBC}_{ijkl} \tag{14}$$

In the case of periodic microstructures, it comes out:

$$\left(S^{SUBC}_{ijkl} \right)^{-1} \leq C^*_{ijkl} = C^{PBC}_{ijkl} = C^{PMUBC}_{ijkl} \leq C^{KUBC}_{ijkl} \tag{15}$$

2.4. Boundary averaging

In the absence of body forces and assuming that the stress field is statically equilibrated, it comes out:

$$\left\langle \sigma_{ij} \right\rangle = \frac{1}{|\Omega|} \int_{\partial\Omega} t_i(\mathbf{x}) \otimes x_j(\mathbf{x}) \; dS \tag{16}$$

$$\left\langle \varepsilon_{ij} \right\rangle = \frac{1}{2|\Omega|} \int_{\partial\Omega} \left(u_i(\mathbf{x}) \otimes n_j(\mathbf{x}) + u_j(\mathbf{x}) \otimes n_i(\mathbf{x}) \right) dS \tag{17}$$

The use of these properties can accelerate dramatically the post-processing of FE output results. They only require the summation of nodal boundary data instead of elementary volumic ones.

3. Test problems

3.1. Problems definition

The first model geometry consists of a single yarn with a circular cross section embedded in a cubic REV (fig. 2). The yarn volumic fraction is set to 0.47. Isotropic materials are used for both the yarn (boron) and the matrix (aluminium) with the following properties: $E_y = 379.3$ GPa, $\nu_y = 0.1$ and $E_m = 68.3$ GPa, $\nu_m = 0.3$. A numerical homogenization procedure is first performed using the conformal FE approach. Thanks to the simplicity of the architecture, the model is generated using Abaqus python scripting language. The convergence of homogenized moduli is studied using 10 nodes tetrahedral (C3D10) and 20 nodes hexahedral (C3D20R - reduced integration) elements. The converged moduli provide accurate references (5 digits) with which voxel-FE results are to be compared (tab. 2, 3).

The second model involves two yarns in a REV of dimensions $(L_1, L_2, L_3) = (6, 6, 4)$ mm. Yarns cross section is elliptic with a major and minor axes of lengths 5 and 1.5 respectively. The geometry is defined in fig. 2. The yarn volumic fraction is $5\pi/32 \approx 0.4909$. The isotropic materials used for the matrix and yarn have the following properties: $E_y = 100$ GPa, $\nu_y = 0.3$ and $E_m = 5$ GPa, $\nu_m = 0.2$. Homogenized elastic moduli are first determined accurately for the model through a convergence study with conformal finite elements (10 nodes tetrahedral C3D10) generated by Abaqus/Python scripts. These moduli may then be used in order to assess the convergence behavior of voxels-FE solutions (tab. 4).

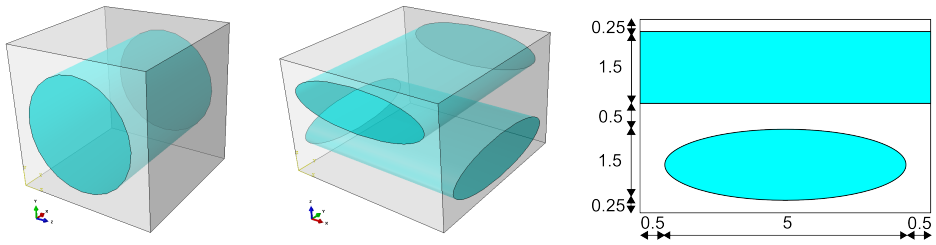

Figure 2. REV used for homogenization procedures : (left) model 1, (center) model 2, (right) model 2 dimensions.

3.2. Convergence analysis

Voxel-FE results are generated with an increasing number of elements using PMUBC. The relative error on moduli decreases as the number of elements increases (tab. 2). These errors have the same behavior as the error on the volumic fraction of yarns. The native voxel mesh overestimates the yarns size and hence their volumic fraction. An option can be specified to the voxelizer software so that a prescribed volumic fraction is satisfied. With this adaptation,

voxel-FE results converge much faster (tab. 3,4 and fig. 3). Examples of deformed REV are provided for model 1 and model 2 under the shear 23 load-case in fig. 4.

n_{DOF} FE-voxel	332k	556k	1.07M	2.11M	5.18M	FEM ref.	VAMUCH [10]
η_{yarn} (%)	51.15	50.02	49.81	49.31	48.34	47	47
E_{11} (GPa)	224,77	224,10	222,54	219,87	219,51	215,33	215,3
E_{22}=E_{33}	153,40	152,43	150,95	148,42	147,91	143,96	144,1
G_{12}=G_{13}	57,90	57,50	56,99	56,09	55,84	54,378	54,39
G_{23}	48,06	47,87	47,51	46,96	46,80	45,823	45,92
$\nu_{12} = \nu_{13}$	0,188	0,188	0,189	0,191	0,192	0,19456	0,195
ν_{23}	0,240	0,241	0,244	0,248	0,248	0,255	0,255

Table 2. Homogenized moduli for model 1 with native voxel-FE PMUBC approach

n_{DOF} FE-voxel	332k	556k	1.07M	2.11M	FEM ref.	VAMUCH [10]
η_{yarn} (%)	47.13	47	47.06	47.11	47	47
E_{11} (GPa)	215.77	215.38	215.55	215.69	215.33	215.3
E_{22}=E_{33}	145.65	145.11	145.11	144.97	143.96	144.1
G_{12}=G_{13}	55.06	54.79	54.74	54.71	54.378	54.39
G_{23}	46.20	46.05	45.97	45.99	45.823	45.92
$\nu_{12} = \nu_{13}$	0.194	0.194	0.194	0.194	0.19456	0.195
ν_{23}	0.250	0.251	0.251	0.252	0.255	0.255

Table 3. Homogenized moduli for model 1 with adapted voxel-FE PMUBC approach

n_{DOF} FE-voxel	222k	422k	715k	1.07M	2.04M	FEM ref.
η_{yarn} (%)	49,26	49,13	49,18	49,06	49,1	49,09
E_{11}=E_{22} (GPa)	34,23	34,11	34,28	34,16	34,14	34.204
E_{33}	12,04	11,90	11,85	11,82	11,77	11.570
G_{12}	7,45	7,39	7,54	7,49	7,44	7.5364
G_{13}=G_{23}	4,64	4,59	4,57	4,57	4,54	4.4692
ν_{12}	0,129	0,129	0,131	0,130	0,130	0.13050
$\nu_{13} = \nu_{23}$	0,245	0,246	0,246	0,247	0,247	0.24957

Table 4. Homogenized moduli for model 2 with adapted voxel-FE PMUBC approach

3.3. Influence of boundary conditions

The first model is submitted to SUBC, PBC, PMUBC and KUBC for different values of the yarn volumic fraction (fig. 5). The voxel-FE models used contains 332k Degrees Of Freedom. The boundings of Eq. (15) are respected. PMUBC and PBC results are in good accordance with reference ones obtained with conformal FE meshes.

4. Conclusion

The numerical homogenization of elastic properties for two material architectures has been successfully performed with voxel-FE models. The reinforcement phase volumic fraction should

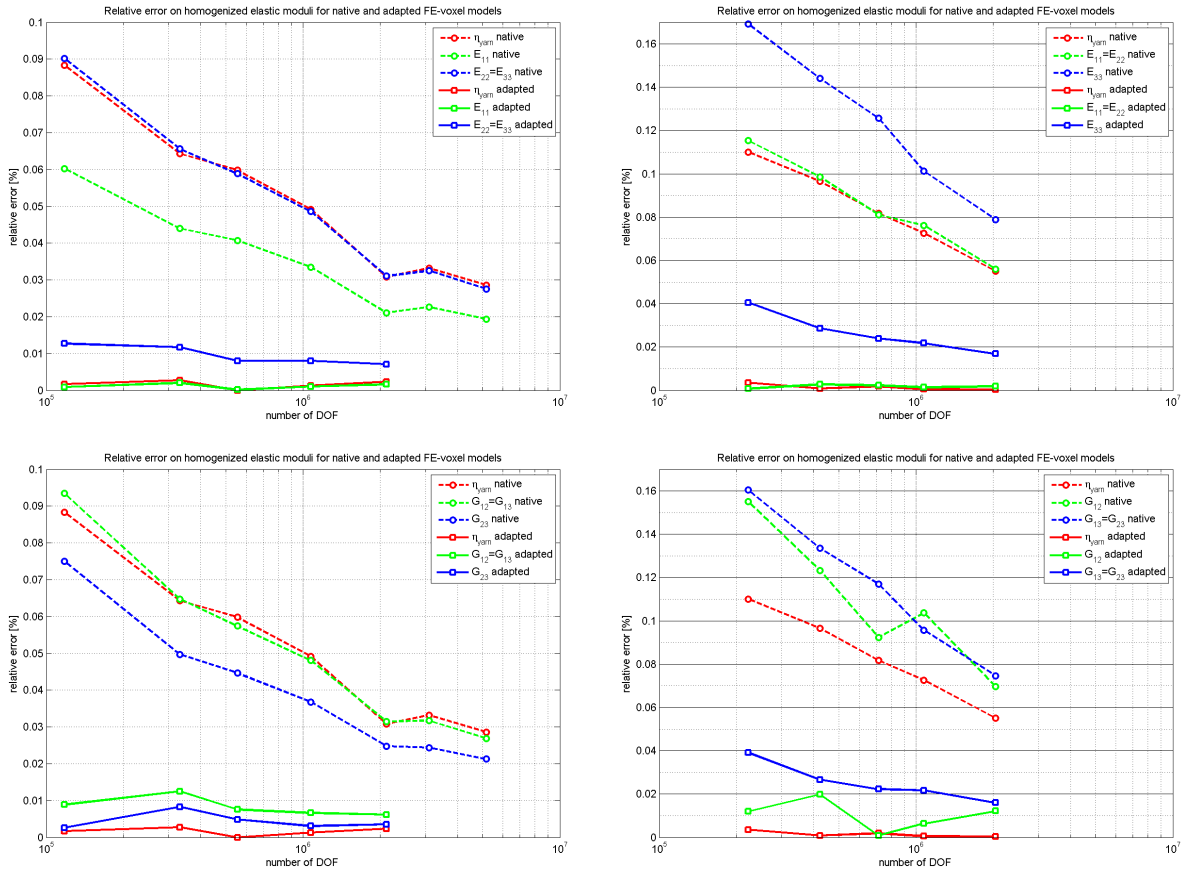

Figure 3. Relative errors on moduli: (left) model 1, (right) model 2.

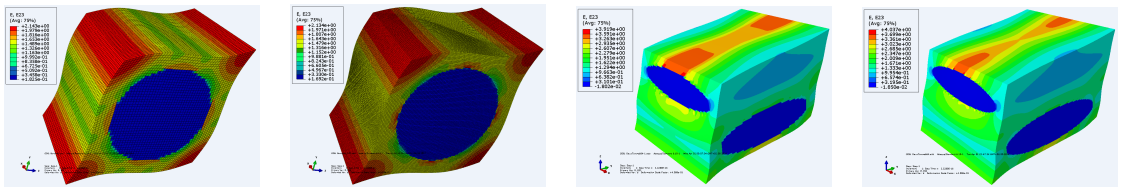

(a) (b) (c) (d)

Figure 4. Deformed shapes of voxel REV under PMUBC shear 23 loading: (a) model 1 with 50^3 voxels, (b) model 1 with 100^3 voxels, (c) model 2 with 50^3 voxels, (d) model 2 with 100^3 voxels.

be specified as an input information so as to reach $\approx 1\%$ accuracy on moduli with relatively light models. Periodic Mixed Uniform Boundary Conditions provide results as accurate as Periodic Boundary Conditions for periodic microstructures.

References

[1] S.V. Lomov, A.V. Gusakov, G. Huysmans, A. Prodromou, and I. Verpoest. Textile geometry preprocessor for meso-mechanical models of woven composites. *Composites Science and Technology*, 60(11):2083 – 2095, 2000.

[2] Stepan V. Lomov, Dmitry S. Ivanov, Ignaas Verpoest, Masaru Zako, Tetsusei Kurashiki,

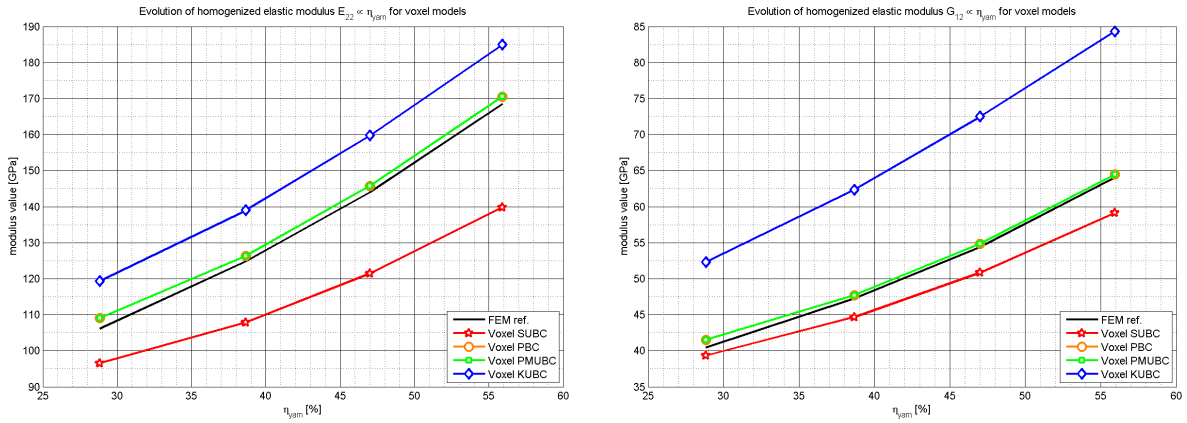

Figure 5. Homogenized elastic moduli for various η_{yarn} using different sets of boundary conditions.

Hiroaki Nakai, and Satoru Hirosawa. Meso-fe modelling of textile composites: Road map, data flow and algorithms. *Composites Science and Technology*, 67(9):1870 – 1891, 2007.

[3] J.J. Crookston, M.N. Sherburn, L.G. Zhao, J.W. Ooi, A.C. Long, and I.A. Jones. Finite element analysis of textile composite unit cells using conventional and novel techniques. In *ICCM15*, 2005.

[4] J. Schneider, G. Hello, Z. Aboura, M. Benzeggagh, and D. Marsal. A meso-FE voxel model of an interlock woven composite. In *17th International Conference on Composite Materials*, 2009. Edinburgh, UK, July 27-31.

[5] G. Hello, A. Tiare, H. Kebir, and Z. Aboura. Finite Elements modeling of mechanical behavior of 3D composite materials. In *15th European Conference on Composite Materials*, 2012. Venice, Italy, June 9-13.

[6] G. Hello, J. Schneider, and Z. Aboura. Generation of voxel-FE models for complex 3D composite architectures. In *8th European Solid Mechanics Conference*, 2012. Graz, Austria, July 9-13.

[7] S.J. Hollister, J.M. Brennan, and N. Kikuchi. A homogenization sampling procedure for calculating trabecular bone effective stiffness and tissue level stress. *Journal of Biomechanics*, 27(4):433 – 444, 1994.

[8] E. Potter, S.T. Pinho, P. Robinson, L. Iannucci, and A.J. McMillan. Mesh generation and geometrical modelling of 3d woven composites with variable tow cross-sections. *Computational Materials Science*, 51(1):103 – 111, 2012.

[9] Dieter H. Pahr and Philippe K. Zysset. Influence of boundary conditions on computed apparent elastic properties of cancellous bone. *Biomechanics and Modeling in Mechanobiology*, 7(6):463–476, 2008.

[10] Wenbin Yu and Tian Tang. Variational asymptotic method for unit cell homogenization of periodically heterogeneous materials. *International Journal of Solids and Structures*, 44(1112):3738 – 3755, 2007.